

# Robust measurement of flexoelectro-optic switching with different surface alignments

Cite as: J. Appl. Phys. **125**, 093104 (2019); <https://doi.org/10.1063/1.5086241>

Submitted: 19 December 2018 . Accepted: 29 January 2019 . Published Online: 04 March 2019

John J. Sandford O'Neill , Julian A. J. Fells , Chris Welch , Georg Mehl , Wing C. Yip, Timothy D. Wilkinson , Martin J. Booth , Steve J. Elston , and Stephen M. Morris 



View Online



Export Citation



CrossMark

## ARTICLES YOU MAY BE INTERESTED IN

[Speckle contrast reduction of laser light using a chiral nematic liquid crystal diffuser](#)  
Applied Physics Letters **109**, 261104 (2016); <https://doi.org/10.1063/1.4971997>

### Ultra High Performance SDD Detectors



See all our XRF Solutions

# Robust measurement of flexoelectro-optic switching with different surface alignments

Cite as: J. Appl. Phys. 125, 093104 (2019); doi: 10.1063/1.5086241

Submitted: 19 December 2018 · Accepted: 29 January 2019 ·

Published Online: 4 March 2019



John J. Sandford O'Neill,<sup>1,a)</sup> Julian A. J. Fells,<sup>1</sup> Chris Welch,<sup>2</sup> Georg Mehl,<sup>2</sup> Wing C. Yip,<sup>3</sup> Timothy D. Wilkinson,<sup>3</sup> Martin J. Booth,<sup>1</sup> Steve J. Elston,<sup>1</sup> and Stephen M. Morris<sup>1,a)</sup>

## AFFILIATIONS

<sup>1</sup>Department of Engineering Science, University of Oxford, Parks Road, Oxford OX1 3PJ, United Kingdom

<sup>2</sup>Department of Chemistry, University of Hull, Hull HU6 7RX, United Kingdom

<sup>3</sup>Department of Engineering, University of Cambridge, Cambridge CB3 0FA, United Kingdom

<sup>a)</sup>Electronic addresses: [john.sandfordoneill@eng.ox.ac.uk](mailto:john.sandfordoneill@eng.ox.ac.uk) and [stephen.morris@eng.ox.ac.uk](mailto:stephen.morris@eng.ox.ac.uk)

## ABSTRACT

The alignment of chiral nematic liquid crystals in the so-called uniform lying helix geometry allows for the observation and exploitation of the flexoelectro-optic effect. However, high-quality uniform lying helix alignment is difficult to achieve reliably, and this can potentially impact the accuracy of the measurements made on the flexoelectro-optic switching behaviour. Here, we show that, using an appropriate method, it is possible to make measurements of the flexo-electric coefficients that are not substantially influenced by the alignment quality.

© 2019 Author(s). All article content, except where otherwise noted, is licensed under a Creative Commons Attribution (CC BY) license (<http://creativecommons.org/licenses/by/4.0/>). <https://doi.org/10.1063/1.5086241>

## I. INTRODUCTION

The molecules that exhibit thermotropic liquid crystal (LC) phases commonly possess a significant electric dipole, which gives rise to the well-known dielectric properties and dielectric anisotropy (the difference between the relative dielectric permittivities parallel and perpendicular to the LC director). This anisotropy in the dielectric properties is exploited in the electro-optic behaviour of most LC-based display technologies. For example, for vertically-aligned nematic technologies, materials are used that consist of molecules with large lateral dipoles, leading to a dielectric permittivity that is larger perpendicular to the director than it is parallel to the director. In contrast, for in-plane switching technologies, the dielectric permittivity parallel to the director constitutes the larger component due to the presence of dipoles that are oriented preferentially along the molecule.

In 1969, Meyer suggested a direct coupling between director distortion and the bulk polarization in LCs through distortion-induced molecular ordering and a consequent ordering of the molecular dipoles.<sup>1</sup> This came to be referred to as “flexoelectricity,” and its interaction with electric fields is commonly designated as the “flexoelectric effect.” The degree of molecular ordering, and therefore the strength of the induced flexoelectric polarization, depends on the LC

director distortion field, which is generally expressed as

$$\mathbf{P}_{flexo} = e_1 \hat{\mathbf{n}}(\nabla \cdot \hat{\mathbf{n}}) + e_3 (\nabla \times \hat{\mathbf{n}}) \times \hat{\mathbf{n}}, \quad (1)$$

where  $\hat{\mathbf{n}}$  is the LC director and  $\mathbf{P}_{flexo}$  is the bulk flexoelectric polarization. The coefficients,  $e_1$  and  $e_3$ , represent the associated flexoelectric coefficients that determine the strength of the induced polarization for splay and bend distortions, respectively, as defined by Meyer.<sup>1</sup>

The flexoelectric effect can manifest in various ways in LC-based technologies. For example, in hybrid-aligned nematic devices, it leads to substantially different electro-optic responses to positive and negative applied electric field pulses.<sup>2</sup> This effect can be exploited in bi-stable systems, such as the zenithally-aligned bi-stable nematic display device.<sup>3</sup> Additionally, flexoelectric effects and the associated dipoles can lead to image-sticking in some display systems.<sup>4</sup>

A potential technology that has received considerable attention in the LC community is that based on the flexoelectro-optic effect in chiral nematic LCs, which was first suggested by Patel and Meyer in 1987.<sup>5</sup> They demonstrated that for a chiral nematic LC with a macroscopic helicoidal structure, there is a coupling between an electric field applied perpendicular to the helical axis and

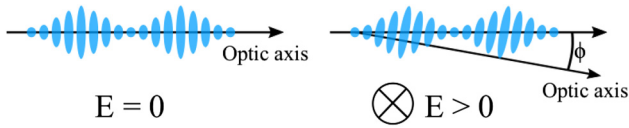


FIG. 1. Illustration of the flexoelectro-optic effect.  $\phi$  is the tilt angle induced by the electric field applied perpendicular to the helix axis.

flexoelectricity that can lead to a rotation of the optic axis around the electric field direction. Moreover, if a thin layer of chiral nematic LC is sandwiched between a pair of glass substrates and is arranged with its helical axis parallel to the substrates, then the application of an electric field between the substrates results in an in-plane reorientation of the macroscopic optic axis.<sup>5</sup> This mechanism is illustrated in Fig. 1.

The in-plane rotation of the optic axis has significant potential since the application of an electric field perpendicular to the substrates allows for direct control of the optic axis of the wave-plate formed by the LC layer (in this case about the electric field direction). Setting the thickness of the LC layer so that it forms a half-wave plate and placing the structure between crossed polarizers then leads to electro-optic behaviour in the form of an intensity modulation (the flexoelectro-optic effect). The electro-optic response time of the helical structure depends on the elastic constants, its viscosity, and also the pitch of the helix.<sup>7</sup> By setting the pitch to be small (i.e., sub-micron), a fast response time of the order of 1 ms can be obtained. This has led to the suggestion in the literature that the electro-optic effect could also be used in fast electro-optic phase modulators.

The flexoelectro-optic effect can be understood in terms of a balance between the electric field coupling to the flexoelectricity and the elastic energy associated with the distortion in the LC. Mathematically, the energy density can be expressed as

$$f = f_{elastic} + f_{flexo} = \frac{1}{2}k_1(\nabla \cdot \hat{n})^2 + \frac{1}{2}k_2[\hat{n} \cdot (\nabla \times \hat{n}) + q_0]^2 + \frac{1}{2}k_3[\hat{n} \times (\nabla \times \hat{n})]^2 - [e_1\hat{n}(\nabla \cdot \hat{n}) + e_3(\nabla \times \hat{n}) \times \hat{n}] \cdot \mathbf{E}, \quad (2)$$

where  $k_1$ ,  $k_2$ , and  $k_3$  are the splay, twist, and bend elastic constants, respectively,  $q_0 = 2\pi/p_0$ , where  $p_0$  is the natural pitch of the helix, and  $\mathbf{E}$  is the applied electric field. The last term in the equation corresponds to the flexoelectric free energy, as defined by Meyer. For the geometry considered here, with the electric field applied perpendicular to the helical axis (which is assumed to be in the  $z$ -direction), the total free-energy can be expressed as<sup>8</sup>

$$f = \frac{1}{2}k_1q^2 \cos^2 qz \sin^2 \phi + \frac{1}{2}k_2[q_0 - q \cos \phi]^2 + \frac{1}{2}k_3q^2 \sin^2 qz \sin^2 \phi - e_1qE \cos^2 qz \sin \phi + e_3qE \sin^2 qz \sin \phi. \quad (3)$$

Here,  $q = 2\pi/p$ , where  $p$  is the actual pitch of the helix,  $\phi$  is the induced tilt angle (see Fig. 1), and  $E$  is the component of the electric field perpendicular to the helix axis.

If it is assumed that the pitch is fixed (does not change under the application of an electric field), then minimization of this free-energy leads to the standard result for the relationship between the tilt angle and the applied electric field,

$$\tan \phi = \frac{(e_1 - e_3)E}{2q_0k_2} - \frac{(k_1 - 2k_2 + k_3)}{2k_2} \sin \phi. \quad (4)$$

For materials with moderate (small angle) responses to applied electric fields, it is then common to approximate the tan and sin terms to the tilt angle, yielding

$$\phi = \frac{(e_1 - e_3)E}{(k_1 + k_3)q_0}, \quad (5)$$

which is typically taken to represent the flexoelectric response of the structure.

In most LC materials, the flexoelectric coefficients are rather small, and hence the tilt angles that can be obtained are limited to only a few degrees. However, it has also been found that for molecules containing a bent core or bimesogenic (dimer) structures, the tilt angles can be large at comparatively low electric field amplitudes.<sup>9-12</sup> In order to exploit the effect fully, it is important to quantify the flexoelectric response of the LC materials. To do this, we need to measure the tilt angle as a function of the applied electric field and then the relevant flexoelectric coefficient combination,  $e_1 - e_3$  in this case, can be determined.

## II. MEASUREMENT OF FLEXOELECTRIC COEFFICIENTS

In order to determine the flexoelectrically-induced tilt angle of the optic axis under an applied electric field, it is generally useful to either (a) directly determine the tilt angle or (b) measure an electro-optic modulation and hence deduce the tilt angle. These methods can be understood if we consider the transmission of a birefringent layer of material (in this case a chiral nematic LC) as a function of angle ( $\chi$ ) when placed between crossed polarizers. In this case, the transmission can be expressed as

$$T(\chi) = \sin^2(2\chi \pm 2\phi) \sin^2 \left\{ \frac{\pi \Delta n_{effective} d}{\lambda} \right\}, \quad (6)$$

where  $\phi$  is the tilt angle in the optic axis as defined in Sec. I,  $\Delta n_{effective}$  is the effective optical anisotropy of the LC,  $d$  is the device thickness, and  $\lambda$  is the wavelength of light. The transmission response as a function of the angle  $\chi$  is shown in Fig. 2.

In order to directly determine the field-induced tilt angle, it is then possible to choose an initial transmission level (such as the 50% level indicated in Fig. 2) and then rotate the LC device to the points where the transmission under the positive applied electric field and the transmission under the negative applied field are equal to the initial transmission. The device rotation is then

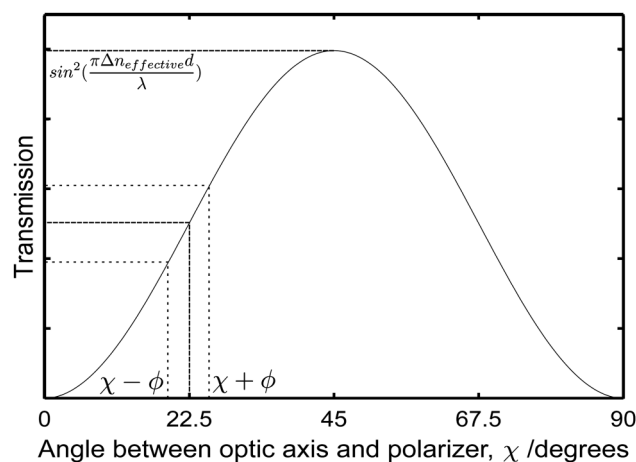


**FIG. 2.** Transmission as a function of the angle between the optic axis and the transmission axis of a polarizer,  $\chi$ , for a flexoelectro-optic LC device sandwiched between crossed polarizers.

equivalent to twice the tilt angle of the optic axis. This measurement method is very convenient and does not require any calibration of the transmission behaviour. However, using this approach, it can be difficult to determine the tilt angle with a sufficiently high degree of accuracy.

Alternatively, it is possible to fix the device angle relative to the transmission axes of the polarizers, and by observing the change in transmission under an applied electric field, the tilt angle can be deduced. At the point indicated in Fig. 2, the “rate of change” of transmission with the tilt angle is given by  $0.5 \sin^2 \left\{ \frac{\pi \Delta n_{\text{effective}} d}{\lambda} \right\}$ . Therefore, by measuring the change in transmission under an applied electric field at this point, it is possible to determine the switching angle for the device under observation. This can be done with a high level of accuracy but can be influenced by non-linearity in the transmission curve shown in Fig. 2. Furthermore, it is also not robust against changes in the optical anisotropy due to field-induced distortions in the helical structure. The reason for this sensitivity is that changes in the effective optical anisotropy, as well as changes in the optic axis orientation, lead to modulation in the transmission under applied electric fields. Despite the shortcomings (i.e., limited accuracy and difficulty in separating the contributions from changes in the optic axis tilt angle from that of birefringence changes), these methods have provided an adequate means of investigating the flexoelectro-optic behaviour and have allowed for the difference in the flexoelectric coefficients,  $e_1 - e_3$  to be determined.

A downside with all these methods is that they typically require a high-quality uniform lying helix (ULH) alignment. The alignment quality can potentially affect the results and non-uniformity in alignment can influence the observed transmission behaviour. Imperfections in the alignment and unwanted light scattering can also change the light levels when the devices are rotated between crossed polarisers. This is additionally exacerbated because in the ULH configuration the alignment is often not ideal and can

be multi-domain in nature. Rotating the device to measure the tilt angle directly can therefore be quite inaccurate. Also, when measuring the modulation, we can see that, in reference to Fig. 2, it is necessary to define and normalize to the maximum transmission. In practice, the maximum and minimum transmissions both need to be determined to allow for offsets, light leakage through the crossed polarizers, etc. In principle, this can be done by rotating the sample, but the alignment and multi-domain issues can again influence the accuracy of the results obtained.

### III. LYING HELIX ALIGNMENT

The alignment of the ULH is challenging because the bulk director profile is not compatible with a simple surface alignment procedure.<sup>13</sup> In well-established LC technologies, the initial bulk director profile is uniform and therefore compatible with a uniform surface alignment. For the case of vertically-aligned switching nematic devices, a homeotropic alignment is used, whereas for the case of in-plane switching systems, a planar alignment is used. However, because of the helical nature of the bulk ULH director profile, this is not immediately compatible with either uniform planar or uniform homeotropic surfaces.

The simplest approach to ULH alignment is to use either a uniform homeotropic or a uniform planar surface and then to induce bulk ULH alignment using additional stimuli, such as induced flow. For example, homeotropic surfaces tend to promote structures with the chiral nematic helix parallel to the substrate surfaces. However, the orientation of the helix axis within the surface plane is not well-defined. For long-pitch chiral nematic LCs, this leads to the fingerprint texture, where the orientation of the helical axis drifts from location to location within the surface plane. Alternatively, for short-pitch chiral nematic LCs, which are of general interest for use in the flexoelectro-optic effect, the variation in the helix axis orientation for homeotropic alignment is over a shorter length-scale. This results in a planar focal-conic-like alignment texture where the helix axis lies in the plane of the device, but the variation in the helix axis orientation manifests in a multi-domain lying helix texture. Subsequently, the application of flow can then break the degeneracy in the helix axis orientation, leading to a more uniform configuration. Using the planar surface alignment, chiral nematic LCs tend to form the Grandjean texture, whereby the helical axis is oriented perpendicular to the surfaces. However, for materials with a positive dielectric anisotropy, the application of an electric field across the device can cause the helical axis to align in the plane of the device. Combining this with flow and/or temperature cycling across the isotropic to chiral nematic phase transition can then result in a situation where the helical axis adopts a more well-defined planar orientation.

In addition to the above processes, there have been a range of other approaches investigated in order to form and stabilize the ULH alignment. For example, periodic surface alignments have been considered, including systems with patterns of homeotropic and planar alignment and a number of differing periodic surface relief structures.<sup>14–17</sup> There have also been investigations of alignment within narrow channels formed between polymer walls, which has resulted in a high-quality alignment with a high optical contrast.<sup>18</sup> The bulk polymer stabilization has also been

shown to ruggedize the ULH alignment, preventing relaxation into the Grandjean texture.<sup>19,20</sup> More recently, studies of ULH alignment within laser-written polymer network systems have been considered.<sup>21</sup> It has also been shown that a very high quality, near mono-domain alignment can be achieved using a solvent evaporation process, although it may be difficult to extend this technique to large areas.<sup>22</sup>

Given the complexity of obtaining a high-quality ULH alignment, together with the limitations imposed by the simple measurement methods outlined above, it can be difficult, or at the very least inconvenient, to establish the flexoelectric coefficient combination,  $e_1-e_3$ . Ideally, a method is needed that works robustly with simple alignments (homeotropic and/or planar) and gives accurate results independent of the precise “quality” of the surface alignment used. The method needs to be able to accurately establish electric field-induced tilt angles, independently from any birefringence changes, and to be able to do so for small signal strengths (small tilt angle changes) even if the ULH structure consists of a multi-domain alignment. Towards this end, we have recently reported a new experimental system for measuring the time-resolved tilt angle

(and retardation) in flexoelectro-optic LC devices,<sup>23</sup> which has the potential to meet these criteria.

#### IV. THE TIME-RESOLVED MEASUREMENT SYSTEM

Consider the system illustrated in Fig. 3(a). The input light can be either left or right circularly polarized, which then passes through a combination of the LC layer and a rotatable polarizer before being incident on a photodetector. If the birefringence of the LC layer is represented by a retardation angle  $\delta$ , where  $\delta = 2\pi\Delta n d/\lambda$ , then the transmission of the system can be expressed as

$$T = \left| \mathbf{P}(\theta)\mathbf{L}(\phi, \delta) \begin{bmatrix} 1/\sqrt{2} \\ \pm i/\sqrt{2} \end{bmatrix} \right|^2 = \frac{1}{2} [1 \pm \sin(2\theta - 2\phi)\sin(\delta)], \quad (7)$$

where  $\mathbf{P}$  is the Jones matrix<sup>24</sup> for the output polarizer at angle  $\theta$ ,  $\mathbf{L}$  is the Jones matrix for the LC layer with optic axis at the switching angle  $\phi$  and the retardation angle  $\delta$ , and the input light is either left or right circularly polarized.

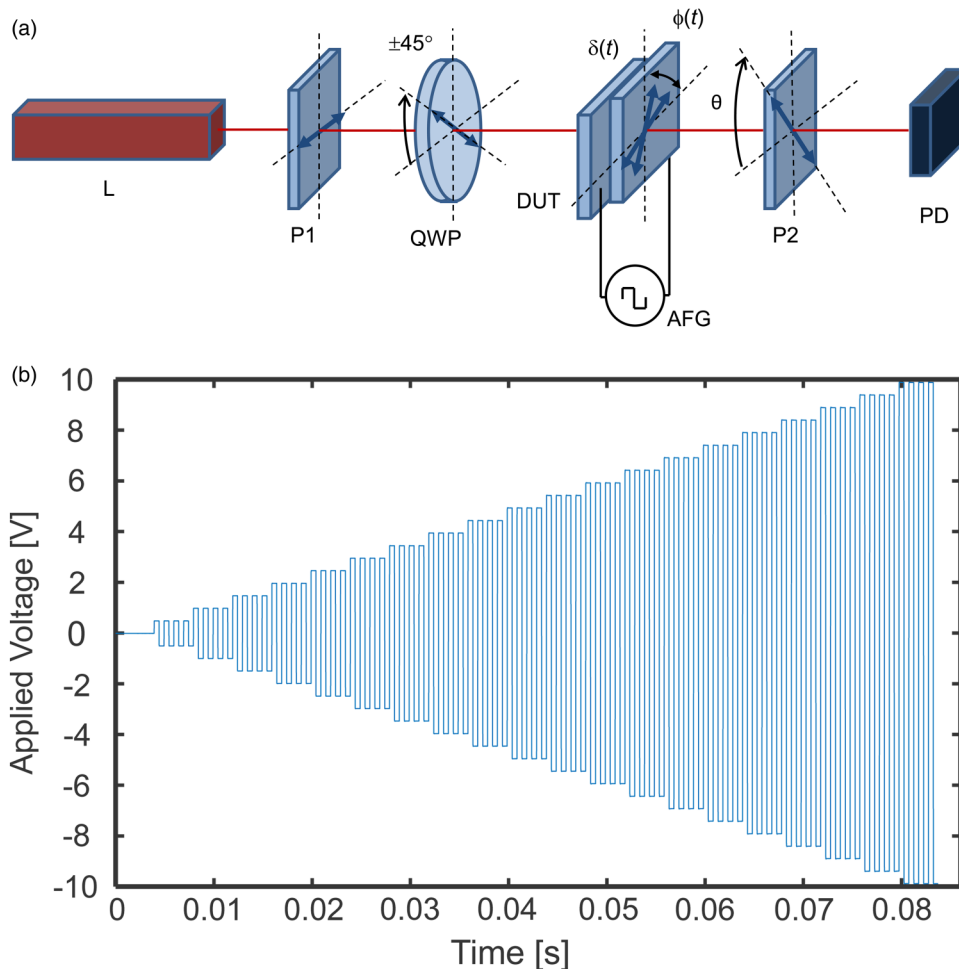
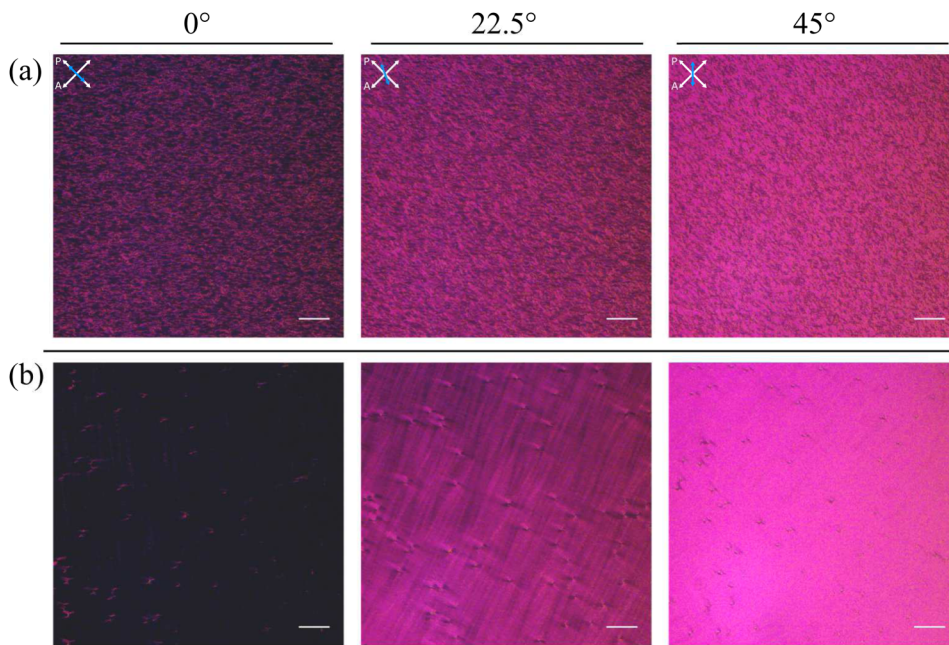


FIG. 3. (a) The experimental arrangement of the measurement system. L: 632.8 nm He-Ne laser, P1: polarizer, QWP: quarter-wave plate, DUT: device under test, AFG: arbitrary function generator, P2: analyzer, PD: photodiode. (b) The voltage signal applied to the flexoelectro-optic LC device in this work.



**FIG. 4.** Polarizing optical microscope images at three different device orientations with respect to the transmission axes of the crossed polarizers ( $0^\circ$ ,  $22.5^\circ$ ,  $45^\circ$ ) for flexoelectro-optic devices consisting of substrate surfaces with anti-parallel rubbed planar alignment layers. (a) Planar anchoring with no flow alignment and (b) planar anchoring with a flow alignment. Devices were filled with the chiral nematic LC mixture consisting of E7 doped with BDH1281 in a  $5\ \mu\text{m}$ -thick device. Measurements were carried out at a temperature of  $25^\circ\text{C}$ . The orientations of the crossed polarizers are indicated by the white arrows and the orientation of the optic axis of the device is indicated by the blue arrows. Scale bars are  $100\ \mu\text{m}$ .

From Eq. (7), we can see that the final transmission through the system as a function of the polarizer angle depends on both the angle of the LC optic axis and the retardation angle (birefringence) of the layer. Therefore, by taking data for  $T(\theta)$ , the amplitude of the resulting function allows for the determination of the retardation angle,  $\delta$ , whereas the phase angle of this function enables the tilt angle,  $\phi$ , of the LC optic axis to be determined. Additionally, it has been shown that by taking data with incident light for both left and right circularly polarized light, it is possible to cancel out any small errors in the polarization state and hence determine  $\delta$  and  $\phi$  with a high degree of accuracy.<sup>23</sup>

Now, let us consider the behaviour of the system if the area under study is broken into a number of sub-domains, each of area  $A_n$  where  $\sum_n A_n = 1$  and where the optic axis of each sub-area is offset by an angle  $\phi_n$  yet switches by  $\phi$ , such that the orientation of the optic axis of the subdomains can be expressed as  $\phi_n + \phi$ . Then, the expression for transmission becomes

$$\begin{aligned}
 T &= \sum_n \frac{1}{2} \{1 \pm \sin[2\theta - 2(\phi_n + \phi)]\sin(\delta)\} A_n \\
 &= \sum_n \frac{1}{2} \{1 \pm [\sin(2\theta - 2\phi)\cos(2\phi_n) \\
 &\quad - \cos(2\theta - 2\phi)\sin(2\phi_n)]\sin(\delta)\} A_n.
 \end{aligned}
 \tag{8}$$

The behaviour of the transmission function given in Eq. (8) is very similar to that represented by Eq. (7). Again, by taking data for  $T(\theta)$ , the phase angle of the resulting function allows for the determination of the LC optic axis tilt angle,  $\phi$ . However, the relationship between the amplitude of the resulting function and the retardation angle,  $\delta$ , is now more complex,

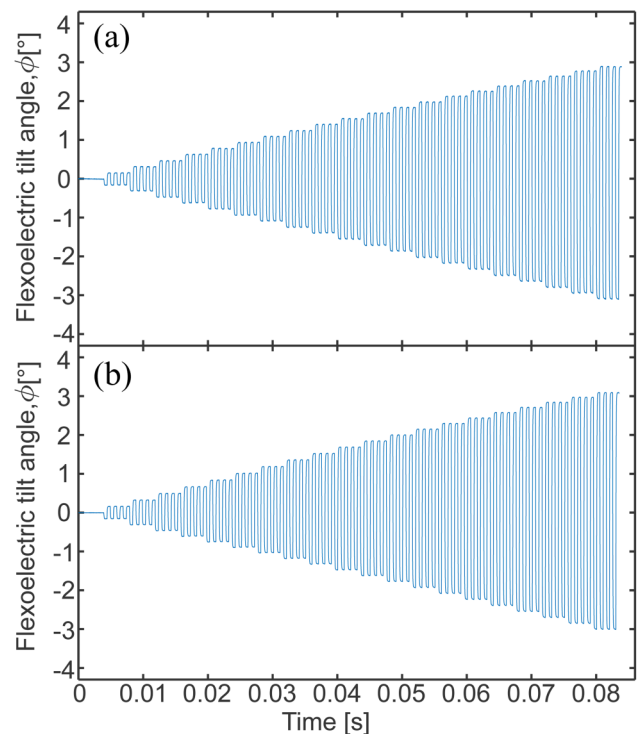


**FIG. 5.** Electric field-induced tilt angle of the optic axis as a function of time for a flexoelectro-optic LC device consisting of the chiral nematic mixture E7 doped with 3.16 wt. % BDH1281. (a) A planar aligned cell with no flow-induced alignment and (b) a planar aligned cell with a flow-induced alignment. Measurements were carried out at  $25^\circ\text{C}$ .

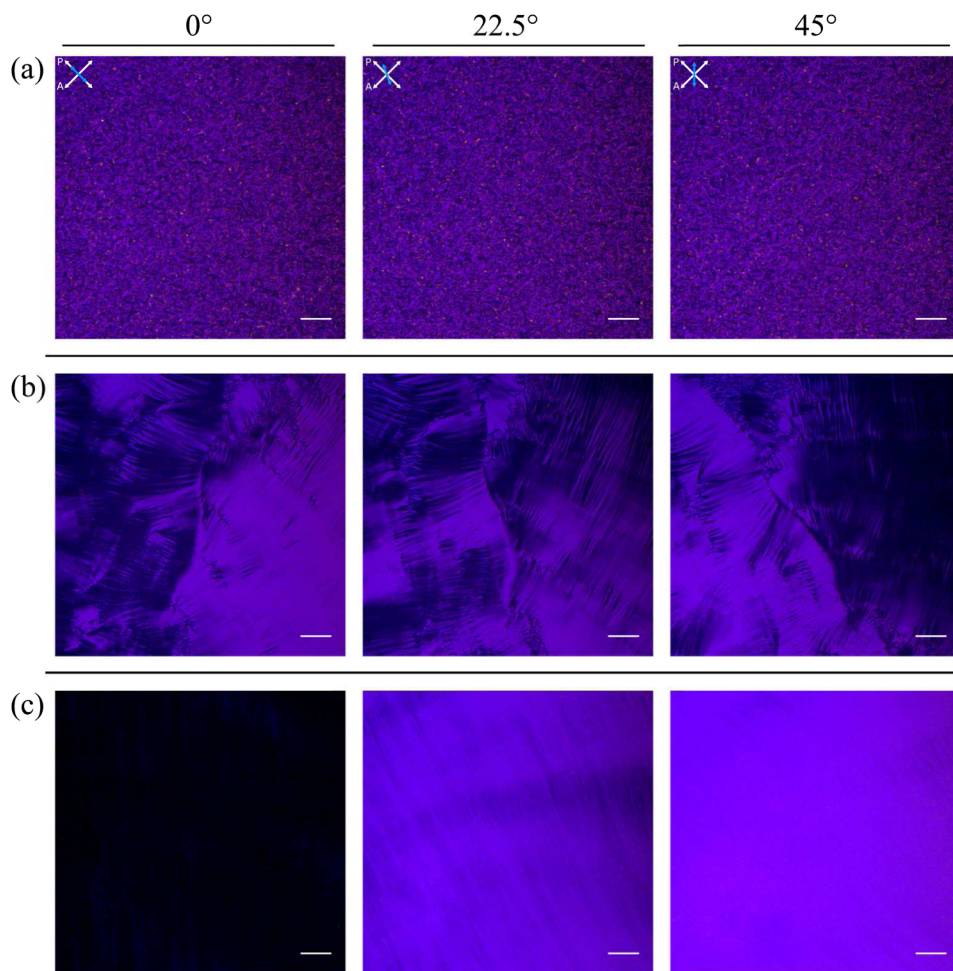


**FIG. 6.** Polarizing optical microscope images at three different device orientations with respect to the transmission axes of the crossed polarizers ( $0^\circ$ ,  $22.5^\circ$ ,  $45^\circ$ ) for flexoelectro-optic devices consisting of substrate surfaces with homeotropic alignment layers. (a) No flow induced (planar focal-conic-like), (b) with some flow induced (multi-domain), (c) with flow induced (near mono-domain). The orientations of the crossed polarizers are indicated by the white arrows and the orientation of the optic axis of the device is indicated by the blue arrows. Scale bars are  $100\ \mu\text{m}$ .

and the retardation cannot be determined without prior knowledge of the sub-domain areas and orientations. This approach is more robust to the non-mono-domain alignment because the LC device itself is not rotated. Therefore, the effects of any non-uniformity, optical scattering, etc. remain constant and do not substantially influence the accuracy of the measurement of the electro-optic tilt angle  $\phi$ .

## V. EXPERIMENTAL METHODS AND SAMPLE PREPARATION

The physical arrangement of the experimental apparatus is shown in Fig. 3(a) and is described in detail elsewhere.<sup>25</sup> The input circular polarization is generated by a combination of a linearly polarized He-Ne laser operating at  $\lambda = 632.8\ \text{nm}$  and a quarter-wave plate. Controlling the axis of the quarter-wave plate allows for the selection of either left or right circular polarization states. The polarizer orientation,  $\theta$ , is rotated in steps and the transmission data are then recorded. Multiplying the data by a sine-function and cos-function (in quadrature) then allows the extraction of the

electro-optic switching angle,  $\phi$ , based on the transmission function presented in Sec. IV [Eq. (8)].

In this study, we use two types of LC device: one with a uniform homeotropic alignment (E.H.C. Co. Ltd) and the other with a uniform planar alignment (Instec Inc.). These are nominally  $5\ \mu\text{m}$ -thick, and each device is filled with a chiral nematic LC mixture consisting of the nematogen mixture E7 (Synthon), doped with the high twisting power chiral additive BDH1281 (Merck) (composition 96.84 wt. % E7 and 3.16 wt. % BDH1281). As a result of using a high twisting power chiral dopant, we only need to add a few wt. % of the BDH1281 and therefore we do not expect a significant change in the flexoelectric coefficients relative to the neat material. The pitch of the resulting chiral nematic LC was found to be  $p = 384\ \text{nm}$  at  $25^\circ\text{C}$  (determined from the transmission spectrum in the Grandjean state recorded on a UV-Vis Spectrometer, A5434—Agilent). The devices were then subsequently treated as described in Sec. VI in order to induce structures with the helix axis in the same plane as the surfaces.

In each case, data were taken by applying a voltage signal of the form illustrated in Fig. 3(b) and were collected over a 1-s window,

which corresponds to a little over six of the pulse sequences shown in the figure. The data were then averaged over the six voltage pulse sequences contained within the 1-s window. The voltage was applied with a Wavetek 195 arbitrary function generator and measurements were taken at 25 °C.

## VI. EXPERIMENTAL RESULTS

### A. Planar surface alignment

The first case we consider is for a device with anti-parallel rubbed surface alignment layers. Initially, an electric field is applied in order to form a structure with the helical axis parallel to the surfaces. No other aligning forces or external stimuli are applied, i.e., we do not induce flow. Without the surface alignment treatment, this process would tend to result in a random planar focal-conic type texture. However, the influence of the surface alignment direction tends to break the degeneracy in the alignment and therefore the helical axis forms with an orientation predominantly along one direction. This is illustrated in Fig. 4(a), which shows the “bright” and “dark” states of the alignment as observed on a polarizing microscope. We can see that one helical axis orientation is dominant, although there is substantial non-uniformity in the overall alignment. Inducing flow in this configuration substantially improves the alignment quality, as seen in Fig. 4(b).

From the electro-optic response obtained for the planar-aligned device, we can extract the electric field-induced flexoelectric tilt angle. This is shown in Fig. 5(a) for the case when there was no flow-induced alignment [corresponding to the alignment texture illustrated in Fig. 4(a)]. We can see that as the amplitude of the electric field is increased, the tilt angle increases, as expected. Additionally, we can see that this response is quite symmetric, indicating that, although the helical axis orientation is not entirely uniform, it is well-defined and stable. The electric field-induced tilt angle for the planar-aligned cell with a flow-induced alignment [corresponding to the alignment texture presented in Fig. 4(b)] is essentially identical to that shown in Fig. 5(a) and is presented in Fig. 5(b). This is an interesting result as it indicates that, although the alignment textures seen in Figs. 4(a) and 4(b) are somewhat different from one another, the measurement system is able to extract reliably the electric field-induced tilt angle in each case, which as expected are found to be the same.

### B. Homeotropic surface alignment

We now consider the case of a device with a homeotropic surface alignment. Initially, we do not induce any flow. To form the alignment, the device is heated and then cooled across the isotropic to chiral nematic phase transition while applying an electric field. In this case, we expect a multi-domain planar focal-conic-like alignment to be formed, and this texture is shown in Fig. 6(a). We can see that in this device there is a uniform but complex texture, and that its appearance is largely independent of the orientation of the device when sandwiched between crossed polarizers—this is the multi-domain planar focal-conic texture. The electro-optic response recorded for this texture is of course very weak. When an electric field is applied, in-plane reorientation of the optic axis may be expected, but different regions tend to “cancel out,” so the overall

response is minimal. That is, in Eq. (8), the  $\phi_n$  values are distributed over the set of areas  $A_n$  so that the overall variation in the transmission as a function of  $\chi$  is thus small.

Despite the weak macroscopic electro-optic behaviour, there is still a small residual response and thus we are able to extract the electric field-induced tilt angle, and this is shown in Fig. 7(a). This response is interesting. Firstly, the fact that we can extract the response shows the sensitivity of the measurement process. Also, although it is broadly similar to that seen in Figs. 5(a) and 5(b) for

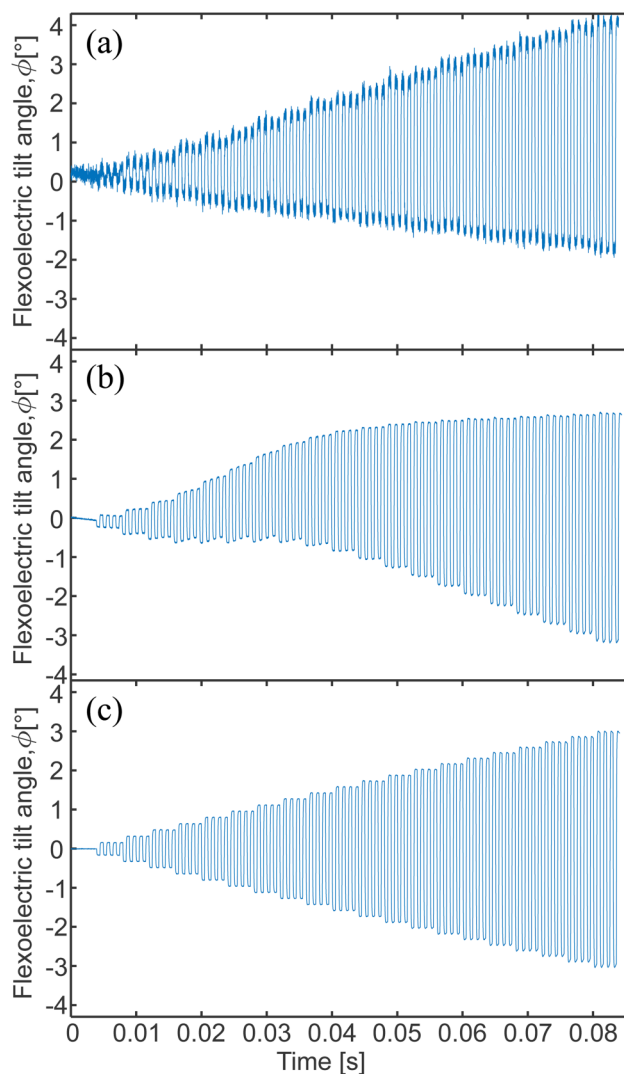


**FIG. 7.** Electric field-induced tilt angle as a function of time for the flexoelectro-optic LC device filled with the chiral nematic mixture of E7 doped with BDH1281 in a 5  $\mu\text{m}$ -thick device. (a) A homeotropic alignment with no flow (planar focal-conic-like), (b) a homeotropic alignment with flow (multi-domain), and (c) a homeotropic alignment with flow (near mono-domain). Measurements were carried out at 25 °C.

the planar-aligned cell, there is now some asymmetry in the response. This indicates that the orientation of the helical axis may not be well-defined and appears to vary with the magnitude of the applied electric field. This could be due to a reorientation of the helical axis under the application of an electric field or it could be because individual areas of sub-domains change when subjected to the electric field, with some sub-domains growing whereas others are shrinking. This would change the effective weighting of the different terms in the summation in Eq. (8) and therefore change the apparent orientation of the optic axis. However, the magnitude of the tilt angle appears to remain well-defined, which will become more evident in Fig. 8.

If we now induce some flow in the homeotropic-alignment device as the texture forms, we can improve the uniformity of the alignment. Such an alignment texture is illustrated in Fig. 6(b). In this case, a small amount of flow has been induced, leading to some alignment, but it remains multi-domain in nature, and there is considerable non-uniformity in the orientation of the helical axis. The resulting tilt angle behaviour is shown in Fig. 7(b), which appears to be very asymmetric, with considerable apparent realignment of the helical axis under the application of an electric field. If we induce further flow in the homeotropic-alignment device to improve the uniformity of the lying helix configuration, the alignment texture illustrated in Fig. 6(c) can now be obtained. This texture shows a near mono-domain alignment, with an appearance similar to or better than that shown in Fig. 4(b). The resulting tilt angle behaviour is shown in Fig. 7(c). This response is now effectively identical to that observed for the planar-aligned device in Fig. 5.

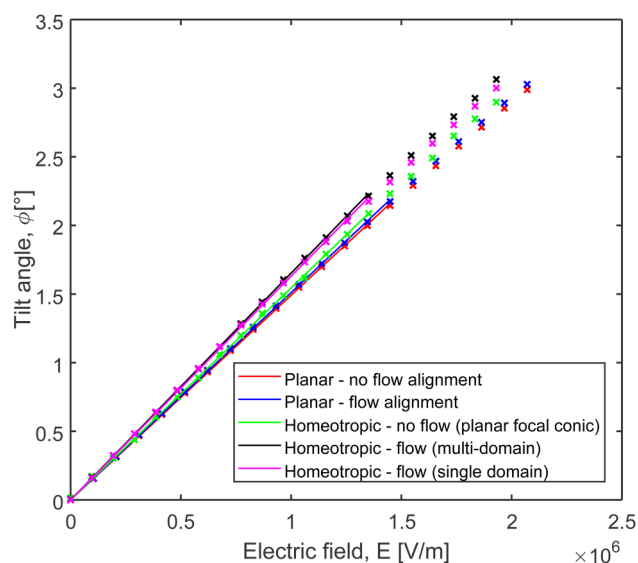


**FIG. 8.** Flexoelectro-optic tilt angle as a function of the applied electric field amplitude for the different alignments of the chiral nematic LC sample consisting of E7+BDH1281 filled into a  $5\mu\text{m}$ -thick cell. The lines are straight-line fits for the linear regime.

**TABLE I.** Measured flexoelectric coefficient combination,  $e_1-e_3$ . The average value is found to be  $12.6 \pm 0.6$  pC/m.

Alignment	$e_1-e_3$ (pC/m)
Planar alignment	12.01
Planar alignment with flow	12.17
Homeotropic alignment (planar focal conic)	12.40
Homeotropic alignment with flow	13.32
Homeotropic alignment near mono-domain	13.14

In order to determine the electric field-induced tilt angles, we now extract the peak-to-peak tilt angles from the results shown in Figs. 5 and 7 and then plot the amplitude of these (half the peak-to-peak values) as a function of the applied electric field. Although there may be some apparent reorientation of the mean helical axis under field application (as clearly seen in some cases in Fig. 7), the amplitudes of the tilt angles remain well defined. The resulting tilt angle behaviour is shown in Fig. 8. As it can be seen, even though the alignment textures differ substantially, the extracted tilt angle behaviour is very similar in each case. These results demonstrate that the measurement method described herein is clearly tolerant to complex multi-domain lying helix alignments and that, even when there may be some apparent field-induced reorientation of the helical axis, it is still possible to extract a well-defined flexoelectro-optic switching behaviour.

Knowledge of the values of  $k_1$  and  $k_3$  for the nematic LC host, E7<sup>25</sup> along with the pitch of the helix for our mixture allows us to extract the flexoelectric coefficients as presented in Table I, which show an average value for  $e_1-e_3$  of  $12.6 \pm 0.6$  pC/m at 25 °C. There have been a number of previous studies and measurements of the difference  $e_1-e_3$  for the nematic LC E7. For example, using a technique involving a hybrid-aligned structure and an in-plane electric field, the value for this difference has been found to be  $e_1-e_3 = 12.7$  pC/m.<sup>26</sup> On the other hand, results using twisted nematic structures have yielded values of  $e_1-e_3 = 9.3$  pC/m and  $e_1-e_3 = 10.6$  pC/m.<sup>25,27</sup> Similarly, work on twisted structures and helical structures have consistently yielded values around  $e_1-e_3 = 12.2$  pC/m.<sup>28-30</sup> While there is some notable variation in the values reported in the literature, the value observed in the current work is consistent with a number of these previous measurements.

## VII. CONCLUSIONS

In this paper, we have demonstrated that a time-resolved measurement method can be used to determine the flexoelectro-optic tilt angle that does not rely on the formation of a high-quality uniform lying helix alignment. This technique has allowed for the determination of the flexoelectric coefficient combination,  $e_1-e_3$ , with consistent values being obtained for alignments ranging from highly uniform (near mono-domain) to highly non-uniform (planar focal-conic-like). The fact that accurate determination of the flexoelectric coefficients can be obtained without requiring a uniform lying helix alignment is very useful because it can be challenging to obtain this alignment and it allows us to “screen” material behaviour in less well-aligned devices. As long as the

helix axis is “lying down” in the plane of the device, it does not matter how many different ULH domains there are, and coefficient values can even be determined when planar focal-conic-like alignment textures are present (i.e., when there is a multi-domain alignment texture where the domains are very small and have randomly oriented helical axes). There is therefore potential for the technique to be used as an efficient method for establishing flexoelectric behaviour of new LC materials without the need to align high quality ULH structures, which is important in the development of new materials that exhibit large tilt angles at moderate voltages and is key to developing new technologies based on the flexoelectro-optic effect.

## ACKNOWLEDGMENTS

J.J.S.O. gratefully acknowledges the Engineering and Physical Sciences Research Council (UK) and Merck for a Graduate Studentship (EP/N509711/1). In addition, the authors also gratefully acknowledge financial support from the Engineering and Physical Sciences Research Council (UK) through Project Nos. EP/M017923/1, EP/M015726/1, and EP/M016218/1.

The research data supporting this publication can be found on the Oxford Research Archive at <https://doi.org/10.5287/bodleian:E9PoQQR49>.

## REFERENCES

- <sup>1</sup>R. B. Meyer, *Phys. Rev. Lett.* **22**, 918 (1969).
- <sup>2</sup>I. Dozov, P. Martinot-Lagarde, and G. Durand, *J. Phys. Lett.* **44**, 817 (1983).
- <sup>3</sup>G. P. Bryan-Brown, E. L. Wood, C. V. Brown, J. C. Jones, I. C. Sage, and P. Brett, *Proc. SID Int. Symp. Digest Tech. Pap.* **28**, 261–264 (1997).
- <sup>4</sup>D. Xu, F. Peng, H. Chen, J. Yuan, S. T. Wu, M. C. Li, S. L. Lee, and W. C. Tsai, *J. Appl. Phys.* **116**, 193102 (2014).
- <sup>5</sup>J. S. Patel and R. B. Meyer, *Phys. Rev. Lett.* **58**, 1538 (1987).
- <sup>6</sup>A. Buka and N. Éber, *Flexoelectricity in Liquid Crystals* (Imperial College Press, 2012).
- <sup>7</sup>J. S. Patel and S. D. Lee, *J. Appl. Phys.* **66**, 1879 (1989).
- <sup>8</sup>P. Rudquist, T. Carlsson, L. Komitov, and S. T. Lagerwall, *Liq. Cryst.* **22**, 445 (1997).
- <sup>9</sup>H. J. Coles, M. J. Clarke, S. M. Morris, B. J. Broughton, and A. E. Blatch, *J. Appl. Phys.* **99**, 1 (2006).
- <sup>10</sup>C. Noot, M. J. Coles, B. Musgrave, S. P. Perkins, and H. J. Coles, *Mol. Cryst. Liq. Cryst.* **366**, 725 (2001).
- <sup>11</sup>P. S. Salter, C. Tschierske, S. J. Elston, and E. P. Raynes, *Phys. Rev. E Stat. Nonlin. Soft Matter Phys.* **84**, 5 (2011).
- <sup>12</sup>A. Varanytsia and L.-C. Chien, *J. Appl. Phys.* **119**, 014502 (2016).
- <sup>13</sup>P. S. Salter, S. J. Elston, P. Raynes, and L. A. Parry-Jones, *Jpn. J. Appl. Phys.* **48**, 1013021 (2009).
- <sup>14</sup>G. Hegde and L. Komitov, *Appl. Phys. Lett.* **96**, 113503 (2010).
- <sup>15</sup>G. Carbone, D. Corbett, S. J. Elston, P. Raynes, A. Jesacher, R. Simmonds, and M. Booth, *Mol. Cryst. Liq. Cryst.* **544**, 37 (2011).
- <sup>16</sup>B. I. Outram and S. J. Elston, *J. Appl. Phys.* **113**, 043103 (2013).
- <sup>17</sup>L. Komitov, G. P. Bryan-Brown, E. L. Wood, and A. B. J. Smout, *J. Appl. Phys.* **86**, 3508 (1999).
- <sup>18</sup>G. Carbone, P. Salter, S. J. Elston, P. Raynes, L. De Sio, S. Ferjani, G. Strangi, C. Umefon, and R. Bartolino, *Appl. Phys. Lett.* **95**, 011102 (2009).
- <sup>19</sup>P. Rudquist, L. Komitov, and S. T. Lagerwall, *Liq. Cryst.* **24**, 329 (1998).
- <sup>20</sup>B. J. Broughton, M. J. Clarke, S. M. Morris, A. E. Blatch, and H. J. Coles, *J. Appl. Phys.* **99**, 023511 (2006).
- <sup>21</sup>C. C. Tartan, P. S. Salter, M. J. Booth, S. M. Morris, and S. J. Elston, *J. Appl. Phys.* **119**, 183106 (2016).
- <sup>22</sup>S. Bolis, C. C. Tartan, J. Beeckman, P. Kockaert, S. J. Elston, and S. M. Morris, *Liq. Cryst.* **45**(5), 774–782 (2018).
- <sup>23</sup>J. A. J. Fells, S. J. Elston, M. J. Booth, and S. M. Morris, *Opt. Express* **26**, 6126 (2018).
- <sup>24</sup>P. Yeh and C. Gu, *Optics of Liquid Crystal Displays* (John Wiley and Sons Ltd, 1999).
- <sup>25</sup>R. A. Ewings, C. Kischka, L. A. Parry-Jones, and S. J. Elston, *Phys. Rev. E Stat. Nonlin. Soft Matter Phys.* **73**, 1 (2006).
- <sup>26</sup>J. H. Wild, K. Bartle, N. T. Kirkman, S. M. Kelly, M. O’Neill, T. Stirner, and R. P. Tuffin, *Chem. Mater.* **17**, 6354 (2005).
- <sup>27</sup>E. K. Tidey, L. A. Parry-Jones, and S. J. Elston, *Liq. Cryst.* **34**, 251 (2007).
- <sup>28</sup>C. Kischka, L. A. Parry-Jones, S. J. Elston, and E. P. Raynes, *Mol. Cryst. Liq. Cryst.* **480**, 103 (2008).
- <sup>29</sup>P. S. Salter, C. Kischka, S. J. Elston, and E. P. Raynes, *Liq. Cryst.* **36**, 1355 (2009).
- <sup>30</sup>B. I. Outram and S. J. Elston, *Liq. Cryst.* **39**, 149 (2012).